15-GHz Epitaxial AlN FBARs on SiC Substrates

Wenwen Zhao, Mohammad Javad Asadi, *Member, IEEE*, Lei Li, *Graduate Student Member, IEEE*, Reet Chaudhuri, Kazuki Nomoto, *Senior Member, IEEE*, Huili Grace Xing, *Fellow, IEEE*, James C. M. Hwang, *Life Fellow, IEEE*, and Debdeep Jena, *Senior Member, IEEE*

***Abstract*— Epitaxial AlN thin-film bulk acoustic resonators (FBARs) on SiC substrates with first-order thickness extensional modes of 15-17 GHz are demonstrated. For the 15 GHz epi-AlN FBARs, the quality factor $Q_{max} \approx 443$, electromechanical coupling coefficient $k^2_{eff} \approx 2.3\%$, and $f \cdot Q \approx 6.65$ *THz* figure of merit achieved are among the highest in the Ku-band (12-18 GHz). A clean primary mode with a high quality factor enables such epi-AlN FBARs to be utilized in Ku-band acoustic filters with clean bands and steep rejection. Because such epi-AlN FBARs share the same SiC substrate and epitaxial growth as AlN/GaN/AlN quantum well high-electron-mobility-transistors (QW HEMTs), they are well suited for monolithic integration with HEMT low noise amplifiers (LNAs) and power amplifiers (PAs).**

***Index Terms*— FBARs, epitaxial, AlN, SiC, super high frequency.**

I. Introduction

HIGH speed communication systems require compact and effective filters in the 6-30 GHz frequency range. [1], [2], [3], [4], [5] These frequencies are beyond the capacity of conventional surface-acoustic wave resonators, and are challenging with bulk acoustic-wave resonators including solidly mounted bulk acoustic resonators (SMRs) and thin-film bulk acoutic resonators (FBARs). FBARs are Metal-Insulator-Metal (M-I-M) structures operating on the principle of energy conversion between electromagnetic and acoustic domains enabled by the piezoelectric (insulating) layer. Neglecting the electrode load, the resonance frequency of the FBAR follows $f = v_s/2L$ with $L \approx \lambda/2$ for the first thickness mode. Here v_s is the longitudinal acoustic velocity in piezoelectric layer and L is the thickness of the piezoelectric layer. Using longitudinal acoustic velocity of AlN $v_s = 11000$ m/s [6] and $L = 300$ nm yields $f \sim 18.3$ GHz. The electrode mass load lowers the resonance frequency of the FBAR from this estimate.

Manuscript received 13 March 2023; accepted 18 April 2023. Date of publication 20 April 2023; date of current version 23 May 2023. This work was supported in part by the Semiconductor Research Corporation (SRC) and the Defense Advanced Research Projects Agency (DARPA) through the Joint University Microelectronics Program (JUMP), carried out in the Cornell NanoScale Facility, a National Nanotechnology Coordinated Infrastructure (NNCI) member partly funded by National Science Foundation (NSF) under Grant NNCI-2025233. The review of this letter was arranged by Editor N. Barniol. *(Corresponding author: Wenwen Zhao.)*

Wenwen Zhao is with the School of Applied and Engineering Physics, Cornell University, Ithaca, NY 14853 USA (e-mail: wz344@cornell.edu).

Mohammad Javad Asadi, Lei Li, Reet Chaudhuri, and Kazuki Nomoto are with the School of Electrical and Computer Engineering, Cornell University, Ithaca, NY 14853 USA.

Huili Grace Xing and Debdeep Jena are with the Department of Materials Science and Engineering, the School of Electrical and Computer Engineering, and the Kavli Institute for Nanoscience, Cornell University, Ithaca, NY 14853 USA.

James C. M. Hwang is with the Department of Materials Science and Engineering, Cornell University, Ithaca, NY 14853 USA.

Color versions of one or more figures in this letter are available at https://doi.org/10.1109/LED.2023.3268863.

Digital Object Identifier 10.1109/LED.2023.3268863

Commercial acoustic filters today normally use sputtered polycrystalline piezoelectric films. Several works successfully extend sputter-material-based FBARs to 10-30 GHz window. [3], [4], [5], [7], [8] By utilizing higher order antisymmetric modes, up to 60 GHz resonance mode with contour mode acoustic resonators have been achieved [9], [10], [11], [12], [13].

Can one leverage the epitaxial AlN layers that are already used for high-speed nitride HEMT amplifiers to realize FBARs without additional sputtering deposition? In this work, we demonstrate such epi-AlN FBARs on SiC substrates operating at the first-order longitudinal mode up to 17 GHz, the highest resonance frequency for epi-FBARs. Without additional material growth, these FBARs can be directly fabricated on the AlN HEMT wafer (e.g. 4 nm thick AlN barrier/30 nm thick GaN channel/ 500 nm thick AlN buffer on the SiC substrate). Fig. 1 benchmarks the resonance frequency and quality factor of III-Nitride FBARs. Higher $f \cdot Q$ within the Akhieser limit and Landau–Rumer (L–R) limit [14], [15] is desired for FBARs. In addition to the high-frequency performance, the $f \cdot Q$ of the 15 GHz highest performance epi-AlN FBARs in this work compare favorably to FBARs operating in the lower 1-6 GHz window for the wireless communication standards of PCS, WCDMA and WiFi.

II. Device Design and Fabrication

Epitaxial AlN thin films were grown on a 3 inch, 100 μm thick semi-insulating 6H-SiC substrate (thinned down from a 350 μm thick substrate) in a Veeco Gen10 plasma-assisted molecular beam epitaxy (MBE) system. An AlN 002 X-ray peak with a 0.1° full width at half maximum (FWHM) rocking curve and a surface rms roughness of 0.26 nm for 5 μm $\times$ 5 μm scan indicate the high crystalline quality of the thin epitaxial AlN films.

Fig. 2(a) shows a 3D schematic of a one-port epi-AlN FBAR on 6H-SiC substrate. Deep SiC etching generates air pockets below AlN and through-SiC-vias (TSVs) below the ground pads. The air pockets suspend the AlN thin film (membrane shown in blue) from the substrate. The TSVs under the ground pads connect the bottom metal on backside of the wafer with the ground pads on topside of the wafer. A series of

0741-3106 © 2023 IEEE. Personal use is permitted, but republication/redistribution requires IEEE permission.
See https://www.ieee.org/publications/rights/index.html for more information.

Authorized licensed use limited to: Cornell University Library. Downloaded on May 24,2023 at 12:25:52 UTC from IEEE Xplore. Restrictions apply.

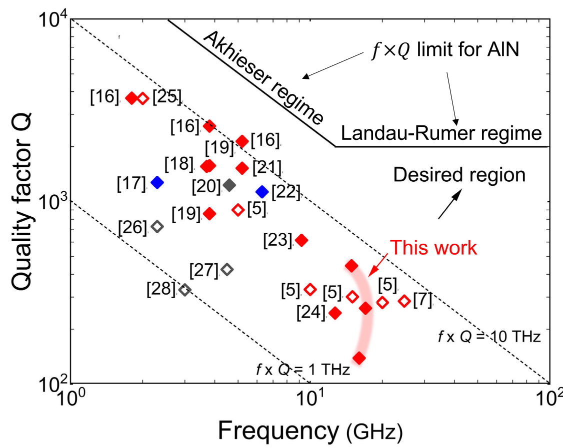

Fig. 1. Benchmark of f and Q_{max} of III-Nitride material BAWs operating with the first-order thickness extensional mode. References [5], [7], [16], [17], [18], [19], [20], [21], [22], [23], [24], [25], [26], [27], [28] Q_S (quality factor at series resonance), instead of Q_{max} of the 24 GHz FBAR in [7] is marked in the benchmark plot since Q_{max} is not stated in the paper.

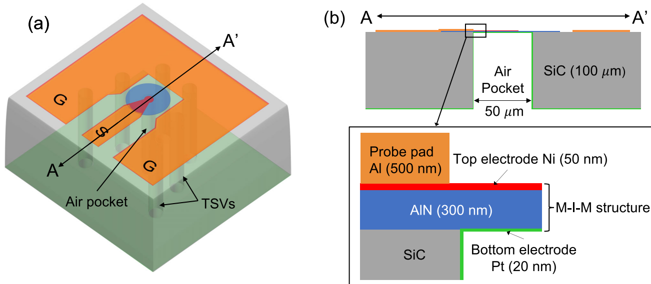

Fig. 2. (a) 3D and (b) 2D cross-sectional conceptual figures an one-port epitaxial AlN FBAR on the SiC substrate. The vibrating region of the FBAR includes an epitaxial AlN layer (blue), a top electrode (red) and a bottom electrode (green).

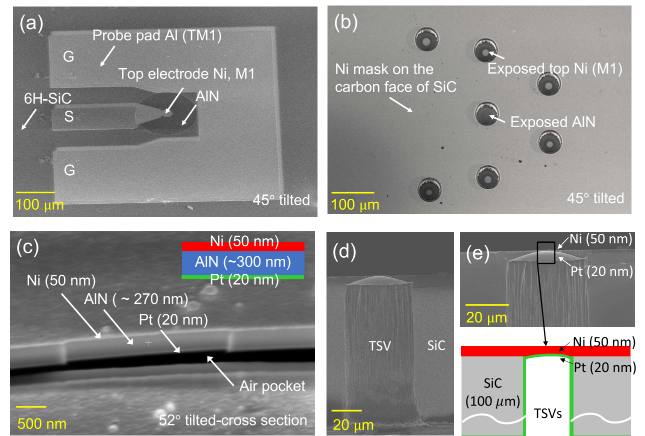

Fig. 3. (a) 45° tilted SEM figure of a fabricated one-port AlN-on-SiC FBAR. (b) 45° tilted backside view of a one-port FBAR after deep SiC etching. (c) 52° tilted SEM figure showing the M-I-M structure of an AlN-on-SiC FBAR. (d) Cross-sectional SEM figure of a TSV under the ground pads. (e) Enlarged SEM figure of (d).

TSVs also help confine the electromagnetic waves. They have a similar function to the vias in substrate integrated waveguides (SIWs). As shown in Fig. 2(b), the electromechanically vibrating region of the FBAR comprises of a top electrode of 50 nm thick Ni, a piezoelectric film of 300 nm thick AlN, and a bottom electrode of 20 nm thick Pt. A 500 nm thick layer of Al was deposited on the probe pads to mitigate metal punch-through due to over-etching of TSVs.

The epi-AlN FBARs in this work used a double-side wafer process. AlN patterning, evaporation of the top electrode and the probe pads are used for top surface. Deep through-SiC etching and ALD deposition of the bottom electrode are performed on the other side. AlN and Ni (M1) are used as the etch stops for the air pockets under AlN and the TSVs under ground pads respectively. In addition to the compatibility with AlN-on-SiC HEMTs, the fabrication of AlN-on-SiC FBARs is also compatible with that of SiC-based substrate integrated waveguides (SIWs) for mm-wave ($\sim$ 140 GHz) frequencies, which require deep through-SiC etching and careful control of etch stop [29].

Fig. 3(a) shows a top view scanning electron microscope (SEM) image of a fabricated one-port AlN FBAR (compare to Fig. 2(a)). Fig. 3(b) shows the SEM image of the backside of the one-port AlN FBAR wafer after deep SiC etching. The exposed topside Ni (M1) is clearly observed due to the contrast between Ni and SiC. The contrast between the exposed AlN and SiC is not sharp, thus Raman spectroscopy was used to confirm that AlN is exposed [23].

To examine the device cross-section, focused ion beam (FIB) cuts were performed on the M-I-M structure on the air pockets. Fig. 3(c) shows a 52° tilted cross section SEM image of the M-I-M structure. The suspended AlN film is $\sim$270 nm thick (over etched by $\sim$ 30 nm) after processing. A clear M-I-M structure indicates the successful SiC etch stop and the deposition of the ultrathin bottom electrodes. Fig. 3(d) and (e), with different magnifications, show the cross section of a TSV under the ground pad. As shown in Fig. 3(e), the bottom electrode Pt contacts the topside Ni, which is the first layer of the probe pad. The TSV is electrically conductive. It is also noted that the bottom of the TSV is tapered. The air pocket has similar tapered shape. [23] The tapered AlN or non-uniform thickness of the AlN layer exhibits unwanted thickness modes close to the main mode. In order to minimize the undesired spurious modes due to non-uniform suspended AlN, the exposed AlN area is minimized to be as small as 10-20 μm in diameter (4-16% of the air pocket area). Ripples in the filter impedance are minimized due to a reduced difference between the center and edge thicknesses of the suspended AlN region. An acceptable DC resistance of 10-17 Ω for the ultra-thin metal (20 nm ALD Pt) coated TSVs was measured with this small contact area of metals from top and back sides.

III. Discussion

Small-signal RF measurements of the FBAR were performed using an Agilent 40 GHz 8722ES vector network analyzer (VNA). After the FBAR measurements, the effects of the measurement cables, and the metal routings on topside of the wafer and the TSVs are de-embedded.

Fig. 4(a) and (b) show the magnitude and phase characteristics of Z_{11} for a one-port 15 GHz AlN FBAR driven by a 50 Ω source. Fig. 4(c) and (d) show the Bode quality factor and the Smith charts of the FBAR in Fig. 4(a) and (b). The Bode quality factor is calculated by $Q(\omega) = 2\pi f \cdot (-d\phi/d\omega) \cdot |S_{11}|/(1-|S_{11}|^2)$. Reference [30] ϕ is the phase

Authorized licensed use limited to: Cornell University Library. Downloaded on May 24,2023 at 12:25:52 UTC from IEEE Xplore. Restrictions apply.

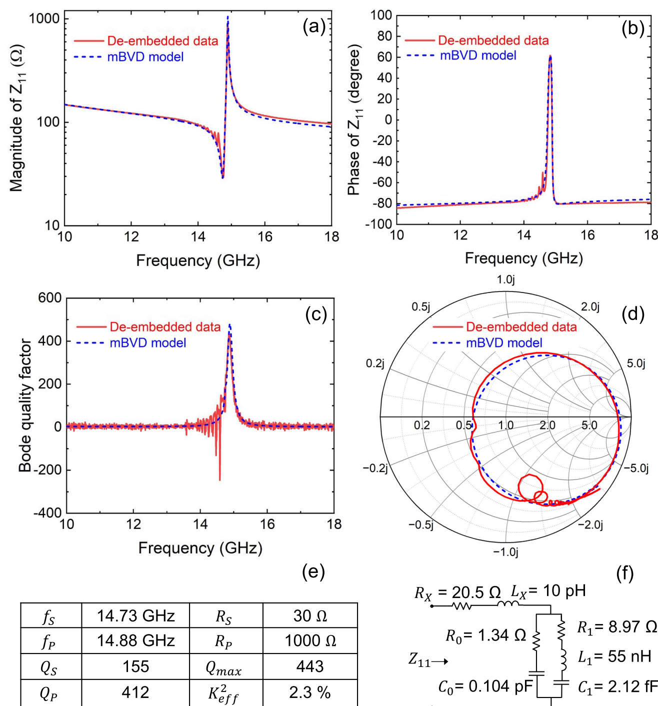

f_S	14.73 GHz	R_S	30 Ω
f_P	14.88 GHz	R_P	1000 Ω
Q_S	155	Q_{max}	443
Q_P	412	K^2_{eff}	2.3 %

Fig. 4. (a) Magnitude plot of Z_{11} of an one-port AlN FBAR driven by a 50 Ω source. (b) Phase plot of Z_{11}, (c) Bode quality factor, (d) Smith charts, (e) parameter sheet and (f) the modified Butterworth-Van-Dyke (mBVD) model of the AlN FBAR in (a).

of S_{11} at a certain frequency f. As shown in Fig. 4(e), the FBAR exhibits a fundamental thickness mode with a series resonance frequency f_s of 14.73 GHz, a parallel resonance frequency f_p of 14.88 GHz, and an electromechanical coupling coefficient $k^2_{eff} \approx 2.3\%$. The resistance at series resonance R_s and the resistance at parallel resonance R_p are 30 Ω and 1000 Ω respectively. A clean and strong resonance with a maximum quality factor $Q_{max} \approx 443$, $Q_s \approx 155$, and $Q_p \approx 412$ around 15 GHz was observed. These promising numbers demonstrate the potential of epitaxial AlN-on-SiC FBARs for high frequency RF filters. A modified Butterworth-Van-Dyke (mBVD) model (as shown in Fig. 4(f)) was extracted based on the measured resonance frequency, quality factor and an estimate of the static capacitance of the FBAR. The mBVD model includes the intrinsic resonator part (R_0, C_0, R_1, L_1, C_1) and the electrode effects (R_X, L_X).

By further etching the AlN layer to 200-250 nm thickness, higher primary resonance mode of 16-17 GHz were realized. Fig. 5(a) and (b) show the magnitude of S_{11} and Smith chart (de-embedded) of additional one-port FBARs operating at 16 GHz ($Q_{max} \approx 139$) and 17 GHz ($Q_{max} \approx 260$). Clear and strong acoustic resonances are observed in Fig. 5(a). These figures indicate successful scaling of epi-AlN FBAR to higher frequencies though more ripples appear around the primary mode and the impedance circle in the Smith chart (Fig. 5(b)) shrinks (the quality factor is lower) compared to the 15 GHz FBARs. The bottom of the TSVs and air pockets is tapered (not perfectly flat) after processing, as indicated in Fig.3 (d) and (e). In this case, the thinnest part of AlN is at the center and the thickest part (possibly with SiC residue) at the edge of the air pocket. The tapered AlN layer generates

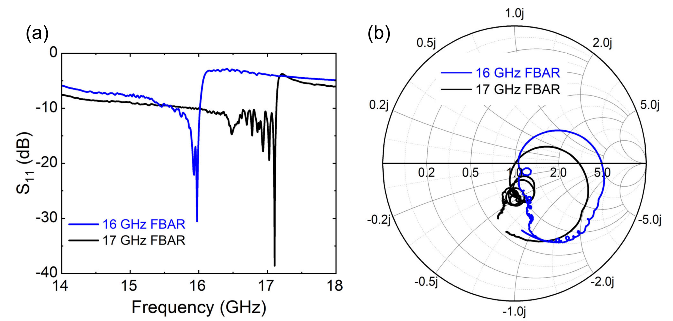

Fig. 5. (a) Magnitude plots of S_{11} and (b) Smith charts for a 16 GHz and a 17 GHz one-port AlN FBAR driven by a 50 Ω source.

thickness modes (ripples.) around the primary mode, as shown in [23]. Another possible explanation for the ripples is the lateral standing waves. Framed electrodes or border rings are widely used to suppress the lateral spurious modes [31].

Over-etching the AlN enlarges the area of exposed AlN which likely induces more ripples due to the non-uniformity of the AlN thickness. At the resonance frequency of the primary mode, the ideal half-wavelength resonance only appears in the region where AlN thickness satisfies the condition for the resonance. The rest of the signal is not injected into the primary mode. Thus a degraded Q of the primary mode is expected. The over-etching of AlN also induces higher resonance frequency. The intrinsic mechanical loss of AlN is represented by $Q_{mech} = v_s^2 \rho/(\omega\eta)$, where v_s is the longitudinal acoustic phase velocity in AlN, ρ is the mass density of AlN, ω is the angular frequency and η is the acoustic viscosity in AlN. [32] The intrinsic Q_{mech} is expected to degrade with higher resonance frequency from the experiment of over-etching.

In order to realize a clean resonance mode at higher frequencies, thinner as-grown epi-AlN (e.g. $<$300 nm) rather than AlN over-etching is needed. However, when the piezoelectric thickness is less than 100 nm (ideally the electrode thickness is roughly 5-10 nm), the electrical loss from electrodes dominates. Epitaxial superconducting electrodes such as NbN, TiN can reduce this load at low temperature and extend the frequency performance of FBARs.

IV. Conclusion

In conclusion, this work has demonstrated epitaxial AlN FBARs on SiC substrates operating at the first order thickness extensional mode of 15-17 GHz with a quality factor over 400, the highest resonance frequencies for epitaxial material based FBARs to date. The figure of merit $f \cdot Q$ of the 15 GHz FBARs is ≈6.65 THz, comparable to single crystalline FBARs operating in 1-6 GHz. The high speed epitaxial AlN FBARs shown here are precursors of monolithic integration of passive acoustic filters and active amplifiers on the SiC substrate.

References

[1] M. Matthaiou, O. Yurduseven, H. Q. Ngo, D. Morales-Jimenez, S. L. Cotton, and V. F. Fusco, "The road to 6G: Ten physical layer challenges for communications engineers," *IEEE Commun. Mag.*, vol. 59, no. 1, pp. 64–69, Jan. 2021, doi: 10.1109/MCOM.001.2000208.

[2] R. Aigner, G. Fattinger, M. Schaefer, K. Karnati, R. Rothemund, and F. Dumont, "BAW filters for 5G bands," in *IEDM Tech. Dig.*, Dec. 2018, pp. 14.5.1–14.5.4, doi: 10.1109/IEDM.2018.8614564.

Authorized licensed use limited to: Cornell University Library. Downloaded on May 24,2023 at 12:25:52 UTC from IEEE Xplore. Restrictions apply.

[3] K. M. Lakin, J. R. Belsick, J. P. McDonald, K. T. McCarron, and C. W. Andrus, "Bulk acoustic wave resonators and filters for applications above 2 GHz," in *IEEE MTT-S Int. Microw. Symp. Dig.*, Jun. 2002, pp. 1487–1490, doi: 10.1109/MWSYM.2002.1012137.

[4] Y. Yoshino, "Piezoelectric thin films and their applications for electronics," *J. Appl. Phys.*, vol. 105, no. 6, Mar. 2009, Art. no. 061623, doi: 10.1063/1.3072691.

[5] K. Umeda, H. Kawamura, M. Takeuchi, and Y. Yoshino, "Characteristics of an AlN-based bulk acoustic wave resonator in the super high frequency range," *Vacuum*, vol. 83, no. 3, pp. 672–674, Oct. 2008, doi: 10.1016/j.vacuum.2008.04.044.

[6] D. Gerlich, S. L. Dole, and G. A. Slack, "Elastic properties of aluminum nitride," *J. Phys. Chem. Solids*, vol. 47, no. 5, pp. 437–441, 1986, doi: 10.1016/0022-3697(86)90039-9.

[7] M. Hara, T. Yokoyama, T. Sakashita, S. Taniguchi, M. Iwaki, T. Nishihara, M. Ueda, and Y. Satoh, "Super-high-frequency band filters configured with air-gap-type thin-film bulk acoustic resonators," *Jpn. J. Appl. Phys.*, vol. 49, no. 7S, Jul. 2010, Art. no. 07HD13, doi: 10.1143/JJAP.49.07HD13.

[8] M. Ueda, M. Hara, S. Taniguchi, T. Yokoyama, T. Nishihara, K.-Y. Hashimoto, and Y. Satoh, "Development of an X-band filter using air-gap-type film bulk acoustic resonators," *Jpn. J. Appl. Phys.*, vol. 47, no. 5, pp. 4007–4010, May 2008, doi: 10.1143/JJAP.47.4007.

[9] Y. Yang, L. Gao, and S. Gong, "X-band miniature filters using lithium niobate acoustic resonators and bandwidth widening technique," *IEEE Trans. Microw. Theory Techn.*, vol. 69, no. 3, pp. 1602–1610, Mar. 2021, doi: 10.1109/TMTT.2021.3049434.

[10] Y. Yang, R. Lu, and S. Gong, "High Q antisymmetric mode lithium niobate MEMS resonators with spurious mitigation," *J. Microelectromech. Syst.*, vol. 29, no. 2, pp. 135–143, Apr. 2020, doi: 10.1109/JMEMS.2020.2967784.

[11] Y. Yang, R. Lu, L. Gao, and S. Gong, "10–60-GHz electromechanical resonators using thin-film lithium niobate," *IEEE Trans. Microw. Theory Techn.*, vol. 68, no. 12, pp. 5211–5220, Dec. 2020, doi: 10.1109/TMTT.2020.3027694.

[12] M. Rinaldi, C. Zuniga, C. Zuo, and G. Piazza, "Super-high-frequency two-port AlN contour-mode resonators for RF applications," *IEEE Trans. Ultrason., Ferroelectr., Freq. Control*, vol. 57, no. 1, pp. 38–45, Jan. 2010, doi: 10.1109/TUFFC.2010.1376.

[13] M. Park, Z. Hao, D. G. Kim, A. Clark, R. Dargis, and A. Ansari, "A 10 GHz single-crystalline scandium-doped aluminum nitride Lamb-wave resonator," in *Proc. 20th Int. Conf. Solid-State Sens., Actuators Microsyst. Eurosensors XXXIII (TRANSDUCERS EUROSENSORS XXXIII)*, Jun. 2019, pp. 450–453, doi: 10.1109/TRANSDUCERS.2019.8808374.

[14] R. Tabrizian, M. Rais-Zadeh, and F. Ayazi, "Effect of phonon interactions on limiting the f.Q product of micromechanical resonators," in *Proc. Int. Solid-State Sens., Actuators Microsyst. Conf. (TRANSDUCERS)*, Jun. 2009, pp. 2131–2134, doi: 10.1109/SENSOR.2009.5285627.

[15] S. A. Chandorkar, M. Agarwal, R. Melamud, R. N. Candler, K. E. Goodson, and T. W. Kenny, "Limits of quality factor in bulk-mode micromechanical resonators," in *Proc. IEEE 21st Int. Conf. Micro Electro Mech. Syst.*, Jan. 2008, pp. 74–77, doi: 10.1109/MEMSYS.2008.4443596.

[16] R. Vetury, M. D. Hodge, and J. B. Shealy, "High power, wideband single crystal XBAW technology for sub-6 GHz micro RF filter applications," in *Proc. IEEE Int. Ultrason. Symp. (IUS)*, Oct. 2018, pp. 206–212, doi: 10.1109/ULTSYM.2018.8580045.

[17] J. B. Shealy, M. D. Hodge, P. Patel, R. Vetury, A. Y. Feldman, S. R. Gibb, M. D. Boomgarden, M. P. Lewis, J. B. Shealy, and J. R. Shealy, "Single crystal AlGaN bulk acoustic wave resonators on silicon substrates with high electromechanical coupling," in *Proc. IEEE Radio Freq. Integr. Circuits Symp. (RFIC)*, May 2016, pp. 103–106, doi: 10.1109/RFIC.2016.7508261.

[18] Y. Aota, Y. Sakyu, S. Tanifuji, H. Oguma, S. Kameda, H. Nakase, T. Takagi, and K. Tsubouchi, "4D-4 fabrication of FBAR for GHz band pass filter with AlN film grown using MOCVD," in *Proc. IEEE Ultrason. Symp.*, Oct. 2006, pp. 337–340, doi: 10.1109/ULTSYM.2006.103.

[19] J. B. Shealy, R. Vetury, S. R. Gibb, M. D. Hodge, P. Patel, M. A. McLain, A. Y. Feldman, M. D. Boomgarden, M. P. Lewis, B. Hosse, and R. Holden, "Low loss, 3.7 GHz wideband BAW filters, using high power single crystal AlN-on-SiC resonators," in *IEEE MTT-S Int. Microw. Symp. Dig.*, Jun. 2017, pp. 1476–1479, doi: 10.1109/MWSYM.2017.8058901.

[20] M. Park, J. Wang, R. Dargis, A. Clark, and A. Ansari, "Super high-frequency scandium aluminum nitride crystalline film bulk acoustic resonators," in *Proc. IEEE Int. Ultrason. Symp. (IUS)*, Oct. 2019, pp. 1689–1692, doi: 10.1109/ULTSYM.2019.8925598.

[21] M. D. Hodge, R. Vetury, S. R. Gibb, M. Winters, P. Patel, M. A. McLain, Y. Shen, D. H. Kim, J. Jech, K. Fallon, R. Houlden, D. M. Aichele, and J. B. Shealy, "High rejection UNII 5.2 GHz wideband bulk acoustic wave filters using undoped single crystal AlN-on-SiC resonators," in *IEDM Tech. Dig.*, Dec. 2017, pp. 25.6.1–25.6.4, doi: 10.1109/IEDM.2017.8268460.

[22] A. Müller, D. Neculoiu, G. Konstantinidis, A. Stavrinidis, D. Vasilache, A. Cismaru, M. Danila, M. Dragoman, G. Deligeorgis, and K. Tsagaraki, "6.3-GHz film bulk acoustic resonator structures based on a gallium nitride/silicon thin membrane," *IEEE Electron Device Lett.*, vol. 30, no. 8, pp. 799–801, Aug. 2009, doi: 10.1109/LED.2009.2023538.

[23] W. Zhao, M. J. Asadi, L. Li, R. Chaudhuri, K. Nomoto, H. G. Xing, J. C. M. Hwang, and D. Jena, "X-band epi-BAW resonators," *J. Appl. Phys.*, vol. 132, no. 2, Jul. 2022, Art. no. 024503, doi: 10.1063/5.0097458.

[24] S. V. Krishnaswamy, J. D. Adam, and M. Aumer, "P1J-4 high-Q FBARs using epitaxial AlN films," in *Proc. IEEE Ultrason. Symp.*, Oct. 2006, pp. 1467–1470, doi: 10.1109/ULTSYM.2006.369.

[25] R. Ruby, R. Parker, and D. Feld, "Method of extracting unloaded Q applied across different resonator technologies," in *Proc. IEEE Ultrason. Symp.*, Nov. 2008, pp. 1815–1818, doi: 10.1109/ULTSYM.2008.0446.

[26] M. Moreira, J. Bjurström, I. Katardjev, and V. Yantchev, "Aluminum scandium nitride thin-film bulk acoustic resonators for wide band applications," *Vacuum*, vol. 86, no. 1, pp. 23–26, 2011, doi: 10.1016/j.vacuum.2011.03.026.

[27] Y. Zou, C. Gao, J. Zhou, Y. Liu, Q. Xu, Y. Qu, W. Liu, J. B. W. Soon, Y. Cai, and C. Sun, "Aluminum scandium nitride thin-film bulk acoustic resonators for 5G wideband applications," *Microsyst. Nanoeng.*, vol. 8, no. 1, p. 124, Nov. 2022, doi: 10.1038/s41378-022-00457-0.

[28] J. Wang, M. Park, S. Mertin, T. Pensala, F. Ayazi, and A. Ansari, "A film bulk acoustic resonator based on ferroelectric aluminum scandium nitride films," *J. Microelectromech. Syst.*, vol. 29, no. 5, pp. 741–747, 2020, doi: 10.1109/JMEMS.2020.3014584.

[29] M. J. Asadi, L. Li, W. Zhao, K. Nomoto, P. Fay, H. G. Xing, D. Jena, and J. C. M. Hwang, "SiC substrate-integrated waveguides for high-power monolithic integrated circuits above 110 GHz," in *IEEE MTT-S Int. Microw. Symp. Dig.*, Jun. 2021, pp. 669–672, doi: 10.1109/IMS19712.2021.9574845.

[30] D. A. Feld, R. Parker, R. Ruby, P. Bradley, and S. Dong, "After 60 years: A new formula for computing quality factor is warranted," in *Proc. IEEE Ultrason. Symp.*, Nov. 2008, pp. 431–436, doi: 10.1109/ULTSYM.2008.0105.

[31] K. Hashimoto, *RF Bulk Acoustic Wave Filters for Communications*. Norwood, MA, USA: Artech House, 2009.

[32] J. Rosenbaum, *Bulk Acoustic Wave Theory and Devices*. Norwood, MA, USA: Artech House, 1988.

Authorized licensed use limited to: Cornell University Library. Downloaded on May 24,2023 at 12:25:52 UTC from IEEE Xplore. Restrictions apply.